Journal Name

ARTICLE TYPE

Cite this: DOI: 10.1039/xxxxxxxxxx

Compositional inhomogeneity and tuneable thermal expansion in mixed-metal ZIF-8 analogues†

Adam F. Sapnik, Harry S. Geddes, Emily M. Reynolds, Hamish H.-M. Yeung,* and Andrew L. Goodwin*

Received Date
Accepted Date

DOI: 10.1039/xxxxxxxxxx

www.rsc.org/journalname

We study the structural and thermomechanical effects of cation substitution in the compositional family of metal–organic frameworks $Zn_{1-x}Cd_x(mIm)_2$ (HmIm = 2-methylimidazole). We find complete miscibility for all compositions x, with evidence of inhomogeneous distributions of Cd and Zn that in turn affect framework aperture characteristics. Using variable-temperature X-ray powder diffraction measurements, we show that Cd substitution drives a threefold reduction in the magnitude of thermal expansion behaviour. We interpret this effect in terms of an increased density of negative thermal expansion modes in the more flexible Cd-rich frameworks.

Mixed-metal and mixed-linker metal–organic frameworks (MOFs) are emerging as an important class of compositionally-complex framework materials,[1–9] favoured for their tuneable catalytic,[10–12] sorption,[13–16] and separation[17] properties. Compositional variation in MOFs is also an attractive method of controlling crystallite morphology[18,19] and even MOF nucleation and growth mechanisms in more general terms.[20] Although there are now many different MOF families in which continuously-variable metal substitution has been demonstrated,[1,6] ZIF-8 is emerging as an especially appealing benchmark system[21] both because its structure is so resilient to substitution and because there are now a number of clear composition–property relationships established for mixed-metal ZIF-8 analogues.[18–20,22,23] By way of example, ethylene/ethane and propylene/propane separation characteristics can be controlled by sequentially substituting Zn^{2+} for Co^{2+} in the ZIF-8 architecture.[17,19,24]

Understanding the structural implications of cation substitution is a particularly important problem for ZIF-8 because so many of its properties—*e.g* sorption characteristics,[25–28] transport properties,[29] phase transition behaviour[30–32] and mechanical stability[30,33]—depend on the geometry and flexibility of its framework structure.[34,35] This structure is related to that of sodalite, except that it is assembled from tetrahedrally-coordinated Zn^{2+} centres and 2-methylimidazolate (mIm^-) linkers [inset to Fig. 1(a)].[21,36] Of the various divalent metals known[37–40] or thought[23] capable of substituting for zinc, it is cadmium that is by far the largest (ionic radii 0.78 *vs* 0.60 Å, Ref. 41) and hence the best placed to influence mechanical properties. While the Cd-containing ZIF-8 analogue $Cd(mIm)_2$ (also known as CdIF-1) has been known for some years,[38] it is only very recently that a mixed-metal Zn/Cd ZIF-8 analogue has been prepared.[22] Given that structural and mechanical sensitivity to compositional variation should be heightened in this particular system, we considered Cd-doped ZIF-8 analogues to offer a particularly exciting platform for tuneable physical behaviour.

Consequently we sought to establish the degree of compositional miscibility of Cd-doped ZIF-8 analogues and to characterise the structural and mechanical consequences of Zn/Cd substitution in this family. Our primary experimental tool is variable-temperature X-ray powder diffraction, but we also exploit a recently-developed[42] non-negative matrix factorisation (NMF) analysis[43,44] of infrared (IR) spectroscopy data to determine compositional correlations in these mixed-metal ZIF-8s.

We prepared a series of eleven ZIF-8 analogues $Zn_{1-x}Cd_x(mIm)_2$ with Cd compositions x spanning the entire range 0 to 1 (see SI for details). Our synthesis followed closely the method reported in Refs. 22 and 38, except that we have used atomic absorption spectroscopy (AAS) as a means of identifying the experimental Zn:Cd ratios in our final samples.[42,45] Despite employing a set of transition-metal precursors with evenly-spaced Cd compositions (x = 0,0.1,0.2,…,1), we found some significant variability between nominal and actual compositions, with $\Delta x = |x_{nom} - x_{exp}| \lesssim 0.1$. In order to establish whether our samples were in fact single-phase mixed-metal ZIF-8

Department of Chemistry, University of Oxford, Inorganic Chemistry Laboratory, South Parks Road, Oxford OX1 3QR, U.K. Tel: +44 (0)1865 272137; E-mail: hamish.yeung@chem.ox.ac.uk or andrew.goodwin@chem.ox.ac.uk

† Electronic Supplementary Information (ESI) available. See DOI: 10.1039/b000000x/

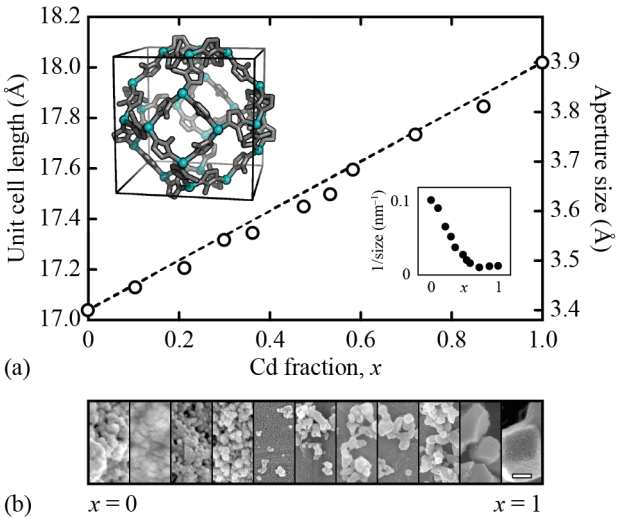

Fig. 1 (a) Compositional dependence of the unit cell length and approximate aperture size in the ZIF-8/CdIF-1 solid solution $Zn_{1-x}Cd_x(mIm)_2$. The dashed line denotes the Vegard limit; error bars are smaller than the symbols. The ZIF-8 structure is represented in the upper inset: Zn atoms as teal spheres and 2-methylimidazolate linkers in grey stick representation. The inverse crystallite size determined by Scherrer analysis is shown in the lower inset. (b) SEM images of the corresponding samples. All images are given at the same magnification: scale bar = 100 nm.

analogues rather than a suitable mixture of ZIF-8 and CdIF-1 with the same overall composition, we used X-ray powder diffraction measurements. We found no evidence of phase segregation, with the diffraction patterns showing a continuous shift in peak positions with varying composition (see SI). Consequently we conclude that the $Zn_{1-x}Cd_x(mIm)_2$ family forms as a continuous isostructural solid solution, which is obviously ideal from the perspective of compositional tuning of physical properties.

Cation substitution is known to have a strong effect on crystallite size and morphology for Co-doped ZIF-8 analogues,[18] and so we used Scherrer analysis of our diffraction data and scanning electron microscopy (SEM) to investigate the distribution of crystallite sizes in our various $Zn_{1-x}Cd_x(mIm)_2$ samples. We found strong parallels to the results of Ref. 18 in the sense that particle size was very small for most of the Zn-rich composition field ($0 < x < 0.7$) but increased rapidly at the very lowest Zn compositions [Fig. 1]. This may be a result of quenching of nanocrystal nucleation processes by soluble Cd-containing complexes—the mechanism proposed for the Co^{2+} case[18]—but we flag also the superior error-correcting properties of Cd^{2+} relative to Zn^{2+} during crystal growth that result from its reduced charge density (*i.e.*, weaker bonding).

In order to determine the structural implication of Cd doping in ZIF-8, we used Pawley refinement of our powder diffraction patterns to determine the compositional dependence of the ZIF-8 unit cell length. Our results are entirely consistent with Vegard-law (*i.e.* linear) behaviour [Fig. 1(a)].[46] The variation we observe in the cubic lattice parameter a of ∼6% is amplified in the variation of the pore aperture dimensions $d \simeq a/2 - 5.1$ Å,[23] such that Cd composition can be used to vary aperture size continuously by as much as 15%. This variability is in strong agreement with the predictions of a recent computational study,[23] and augers well for the eventual use of Cd-doped ZIF-8 analogues as highly-selective porous media.

While unit cell dimensions provide a measure of structure that is representative of the ensemble average, the dimensions of individual pore apertures will be influenced by their microscopic composition. For example, transport in sodalite framework materials is heavily influenced by the structure of the 4-rings,[47] each of which can correspond to any one of five different compositions in Cd-doped ZIF-8 analogues: Zn_4, Zn_3Cd, Zn_2Cd_2, Cd_3Zn, and Cd_4. 4-rings of these different compositions will have varying affinities for guest molecules, and hence control over the relative populations of 4-ring compositions provides a mechanism for tailoring host–guest interactions in mixed-metal ZIF-8. The relative distributions of these different aperture types will be affected by compositional correlations, which we sought to characterise in our samples. In order to do so, we employed a recently-developed IR/NMF approach which exploits the sensitivity of linker vibrational frequencies to the chemical nature of the metals to which linkers are bound.[42] The in-plane mIm bending region of the IR absorption spectrum of $Zn_{1-x}Cd_x(mIm)_2$ is an excellent candidate for this type of analysis, since one expects distinct signatures for bending modes of Zn–mIm–Zn, Zn–mIm–Cd, and Cd–mIm–Cd linkages.[48]

Our experimental IR measurements show a continuous evolu-

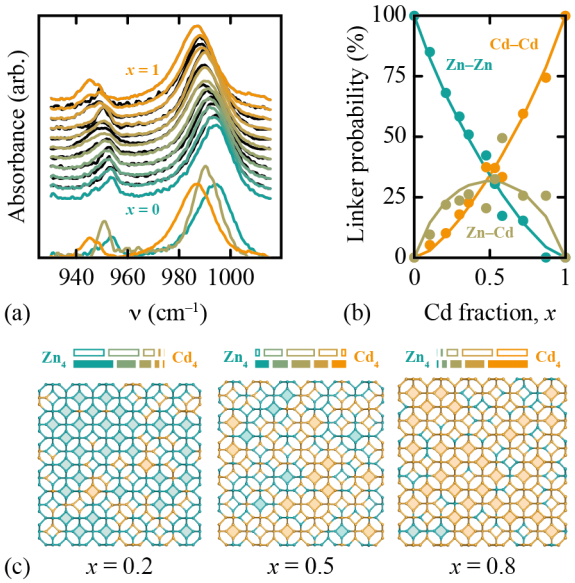

Fig. 2 (a) IR absorption spectra (black lines) and NMF fits (coloured lines) for the in-plane bending region of our $Zn_{1-x}Cd_x(mIm)_2$ samples. Successive data sets are offset by a constant absorbance. The NMF components are shown at the bottom of the plot, and correspond to in-plane bending modes of three linker types: Zn–mIm–Zn (teal), Zn–mIm–Cd (gold), and Cd–mIm–Cd (orange). (b) Linker probabilities extracted from NMF fits to the IR data of (a) are shown as filled circles, and the corresponding best-fit equilibrium distribution model shown as solid lines. (c) Representative sections of RMC configurations driven by the IR-derived equilibrium model described in the text. Homometallic 4-rings are shaded in teal (Zn) and orange (Cd). The fractional population of Zn_nCd_{4-n} 4-rings is shown in bar representation above each section for (top, open bars) statistical and (bottom, filled bars) experimental distributions.

tion in absorption profile with composition x [Fig. 2(a)]. These data cannot be interpreted satisfactorily in terms of linear combinations of the endmember IR traces, implying the presence of Zn–mIm–Cd linkages in mixed-metal $Zn_{1-x}Cd_x(mIm)_2$ and hence substantial mixing on the atomic scale. Following the approach of Ref. 42 we used NMF analysis to extract the best-fit Zn–mIm–Cd trace and, in turn, the relative probabilities of the three linker types as a function of sample composition [Fig. 2(b)]. The NMF algorithm seeks to describe the ensemble of experimental IR traces in terms of linear combinations of three components: two components are the IR traces for the Zn- and Cd-containing endmembers, and the third—which we interpret as the trace arising from vibrations of Zn–mIm–Cd linkages—is allowed to vary in order to best fit the data. The component weights are free variables in our NMF fit, but are subject to two constraints: namely, that the weight sum is unity, and that mass balance is preserved.

The variation in linker probability with cation substitution that we determine [Fig. 2(b)] is somewhat less smooth than that measured for mixed-metal formates.[42] Nevertheless we can interpret these data in terms of an equilibrium model with $\Delta H_{mix} \simeq -RT\ln(K/2) = 1.9(4)\,kJ\,mol^{-1}$.[42] Here, K is the equilibrium constant for the system $\frac{1}{2}$Zn–Zn + $\frac{1}{2}$Cd–Cd $\rightleftharpoons$ Zn–Cd, where M–M denotes a M–mIm–M linkage; we find $K = 0.93$ gives the best fit to the NMF-extracted linker probabilities. The key point is that ΔH_{mix} is clearly > 0, which implies a tendency for homometallic clustering and hence compositional heterogeneities within $Zn_{1-x}Cd_x(mIm)_2$ samples.‡ In turn, the relative distribution of 4-ring compositions (and hence aperture dimensions) is necessarily different to the statistical ($\Delta H_{mix} = 0$; $K = 2$) case. We note that NMR measurements may provide a useful alternative measure of local compositional ordering, as has been applied recently to the related problem of linker distributions in mixed-linker MOFs.[49–51]

To investigate this point further, we used the same reverse Monte Carlo (RMC[52]) approach of Ref. 42 to generate atomistic configurations of $Zn_{1-x}Cd_x(mIm)_2$ structures with Cd/Zn distributions informed by our IR/NMF analysis. As expected, we find that homometallic 4-rings (Zn_4 or Cd_4) are significantly more predominant at all compositions than would be expected if Cd and Zn centres were distributed randomly [Fig. 2(c)]. While linker clustering has been demonstrated using ^{1}H NMR spectroscopy for mixed-ligand ZIF-8 analogues (*e.g.* the ZIF-8/ZIF-90 series[50]), we believe this is the first experimental characterisation of nonuniform metal distributions in a mixed-metal ZIF-8 series.[19]

But what of the effect of Cd doping in $Zn_{1-x}Cd_x(mIm)_2$ on framework flexibility? Thermal expansion behaviour is a straightforward experimental metric of flexibility in framework materials since it is influenced heavily by low-energy lattice modes that often have negative thermal expansion (NTE; volume contraction on heating) characteristics.[34,53] Increasing framework flexibility

‡ Note that the alternate case $\Delta H_{mix} < 0$ implies local Zn/Cd order that gives rise to characteristic diffuse scattering at points in reciprocal space allowed for the $P\bar{4}3n$ space group of *e.g.* $LiB(mIm)_4$ and $CuB(mIm)_4$ (Ref. 37) but forbidden in the $I\bar{4}3m$ space group of ZIF-8. We do not observe any such scattering for $Zn_{1-x}Cd_x(mIm)_2$ at any composition x.

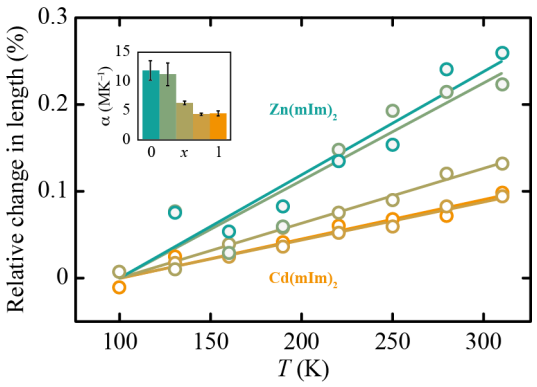

Fig. 3 Thermal expansion behaviour of $Zn_{1-x}Cd_x(mIm)_2$ as determined using variable-temperature X-ray powder diffraction measurements. Data are shown for five compositions (top–bottom): x = 0.0, 0.30, 0.47, 0.58, and 1.0. The inset shows the compositional dependence of the linear coefficient of thermal expansion α.

usually increases the influence of NTE modes, such that the coefficient of thermal expansion becomes more negative as linker length is increased[54,55] and/or bond strengths are reduced.[56] By repeating our X-ray powder diffraction measurements at various temperatures over the range $100 \leq T \leq 310$ K, we were able to determine coefficients of thermal expansion for a subset of our $Zn_{1-x}Cd_x(mIm)_2$ samples. Our data show linear thermal expansion behaviour for all compositions, with a continuous and monotonic decrease in coefficient of thermal expansion $\alpha = (\partial a/a\partial T)_p$ as a function of increasing Cd content [Fig. 3]: α spans the values 11.9(17) MK^{-1} for $x = 0$ to 4.5(4) MK^{-1} for $x = 1$.

So we conclude that Cd doping in ZIF-8 renders the framework structure increasingly flexible (*i.e.* stronger NTE characteristics), which we attribute to the weaker bonding in Cd–mim *vs* Zn–mIm interactions. This difference in bond strength has been noted previously in the context of mechanical amorphisation of ZIF-8 and CdIF-1,[57] is reflected in the empirical force fields of Ref. 23, and (in another guise) plays a role in the stronger NTE behaviour of $Cd(CN)_2$ *vs* $Zn(CN)_2$.[58–60] What is particularly attractive here is that the continuous miscibility of Cd and Zn in ZIF-8 allows for genuine compositional tuning of thermomechanical response. Moreover we find that compositional variation can be used to tune thermal expansion by a factor of three in this family. The additional ability of ZIF-8 to support non-random cation distributions opens up the appealing possibility of correlated disorder tuning[61–63] *via* variation in *e.g.* synthesis temperature. The effect of compositional correlations on mechanical properties, guest sorption and separation profiles then offers an obvious and appealing avenue of further research.

Acknowledgements

The synchrotron diffraction measurements were carried out at the Diamond Light Source (I11 Beamline). We are extremely grateful for the award of a Block Allocation Grant, which made this work possible, for the assistance in data collection provided by Dr Claire Murray (Diamond) and the I11 beamline staff. The authors also thank Hanna Boström (Oxford) and Jonas Bruckmoser (TU Munich) for assistance with AAS measurements, and Jen-

nifer Holter (Oxford) for assistance with SEM measurements. We acknowledge financial support from the E.P.S.R.C. (studentship to H.S.G.) and the Glasstone Trust (fellowship to H.H.M.Y.). This project received funding from the European Union (EU) Horizon 2020 Research and Innovation Programme under Marie Sklodowska-Curie Grant Agreement 641887 (project acronym DEFNET).

Conflict of interest

There are no conflicts to declare.

References

1 A. D. Burrows, *Cryst. Eng. Comm.*, 2011, **13**, 3623–3642.
2 R. Haldar and T. K. Maji, *Cryst. Eng. Comm.*, 2013, **15**, 9276–9295.
3 H. Furukawa, U. Müller and O. M. Yaghi, *Angew. Chem. Int. Ed.*, 2015, **54**, 3417–3430.
4 Z. Fang, B. Bueken, D. De Vos and R. A. Fischer, *Angew. Chem. Int. Ed.*, 2015, **54**, 7234–7254.
5 A. K. Cheetham, T. D. Bennett, F.-X. Coudert and A. L. Goodwin, *Dalton Trans.*, 2016, **45**, 4113–4126.
6 T. D. Bennett, A. K. Cheetham, A. H. Fuchs and F.-X. Coudert, *Nature Chem.*, 2017, **9**, 11–16.
7 J. Ren, M. Ledwaba, N. M. Musyoka, H. W. Langmi, M. Mathe, S. Liao and W. Pang, *Coord. Chem. Rev.*, 2017, **349**, 169–197.
8 J.-S. Qin, S. Yuan, Q. Wang, A. Alsalme and H.-C. Zhou, *J. Mater. Chem. A*, 2017, **5**, 4280–4291.
9 A. Helal, Z. H. Yamani, K. E. Cordova and O. M. Yaghi, *Natl. Sci. Rev.*, 2017, **4**, 296–298.
10 A. Dhakshinamoorthy, A. M. Asiri and H. Garcia, *Catal. Sci. Technol.*, 2016, **6**, 5238–5261.
11 A. Schejn, A. Aboulaich, L. Balan, V. Falk, J. Lalevèe, G. Medjahdi, L. Aranda, K. Mozet and R. Schneider, *Catal. Sci. Technol.*, 2015, **5**, 1829–1839.
12 Q. Liu, H. Cong and H. Deng, *J. Am. Chem. Soc.*, 2016, **138**, 13822–13825.
13 J.-S. Qin, D.-Y. Du, W.-L. Li, J.-P. Zhang, S.-L. Li, Z.-M. Su, X.-L. Wang, Q. Xu, K.-Z. Shao and Y.-Q. Lan, *Chem. Sci.*, 2012, **3**, 2114–2118.
14 J. A. Thompson, C. R. Blad, N. A. Brunelli, M. E. Lydon, R. P. Lively, C. W. Jones and S. Nair, *Chem. Mater.*, 2012, **24**, 1930–1936.
15 J. A. Thompson, N. A. Brunelli, R. P. Lively, J. R. Johnson, C. W. Jones and S. Nair, *J. Phys. Chem. C*, 2013, **117**, 8198–8207.
16 G. Kaur, R. K. Rai, D. Tyagi, X. Yao, P.-Z. Li, X.-C. Yang, Y. Zhao, Q. Xu and S. K. Singh, *J. Mater. Chem. A*, 2016, **4**, 14932–14938.
17 C. Wang, F. Yang, L. Sheng, J. Yu, K. Yao, L. Zhang and Y. Pan, *Chem. Comm.*, 2016, **52**, 12578–12581.
18 J. K. Zaręba, M. Nyk and M. Samoć, *Cryst. Growth Design*, 2016, **16**, 6419–6425.
19 F. Hillman, J. M. Zimmerman, S.-M. Paek, M. R. A. Hamid, W. T. Lim and H.-K. Jeong, *J. Mater. Chem. A*, 2017, **5**, 6090–6099.
20 D. Saliba, M. Ammar, M. Rammal, M. Al-Ghoul and M. Hmadeh, *J. Am. Chem. Soc.*, 2018, **140**, 1812–1823.
21 K. S. Park, Z. Ni, A. P. Côté, J. Y. Choi, R. Huang, F. J. Uribe-Romo, H. K. Chae, M. O'Keeffe and O. M. Yaghi, *Proc. Natl. Acad. Sci., U.S.A.*, 2006, **103**, 10186–10191.
22 J. Sun, L. Semenchenko, W. T. Lim, M. F. Ballesteros Rivas, V. Vaerla-Guerrero and H.-K. Jeong, *Micro. Meso. Mater.*, 2018, **264**, 35–42.
23 P. Krokidas, S. Moncho, E. N. Brothers, M. Castier and I. G. Economou, *Phys. Chem. Chem. Phys.*, 2018, **20**, 4879–4892.
24 P. Krokidas, M. Castier, S. Moncho, D. N. Sredojevic, E. N. Brothers, H. T. Kwon, H. K. Jeong, J. S. Lee and I. G. Economou, *J. Phys. Chem. C*, 2016, **120**, 8116–8124.
25 C. O. Ania, E. García-Pérez, M. Haro, J. J. Gutiérrez-Sevillano, T. Valdés-Solís, J. B. Parra and S. Calero, *J. Phys. Chem. Lett.*, 2012, **3**, 1159–1164.
26 D. Fairen-Jimenez, R. Galvelis, A. Torrisi, A. D. Gellan, M. T. Wharmby, P. A. Wright, C. Mellot-Draznieks and T. Düren, *Dalton Trans.*, 2012, **41**, 10752–10762.
27 H. Tanaka, S. Oshaki, S. Hiraide, D. Yamamoto, S. Watanabe and M. T. Miyahara, *J. Phys. Chem. C*, 2014, **118**, 8445–8454.
28 C. L. Hobday, C. H. Woodall, M. J. Lennox, M. Frost, K. Kamenev, T. Düren, C. A. Morrison and S. A. Moggach, *Nature Commun.*, 2018, **9**, 1429.
29 E. Haldoupis, T. Watanabe, S. Nair and D. S. Sholl, *Chem. Phys. Chem.*, 2012, **13**, 3449–3452.
30 K. W. Chapman, G. J. Halder and P. J. Chupas, *J. Am. Chem. Soc.*, 2009, **131**, 17546–17547.
31 S. A. Moggach, T. D. Bennett and A. K. Cheetham, *Angew. Chem. Int. Ed.*, 2009, **48**, 7087–7089.
32 C. L. Hobday, T. D. Bennett, D. Fairen-Jimenez, A. J. Graham, C. A. Morrison, D. R. Allan, T. Düren and S. A. Moggach, *J. Am. Chem. Soc.*, 2018, **140**, 382–387.
33 S. Cao, T. D. Bennett, D. A. Keen, A. L. Goodwin and A. K. Cheetham, *Chem. Commun.*, 2012, **48**, 7805–7807.
34 F.-X. Coudert, *Chem. Mater.*, 2015, **27**, 1905–1916.
35 F.-X. Coudert, *Chem. Phys. Chem.*, 2017, **18**, 2732–2738.
36 R. Banerjee, A. Phan, B. Wang, C. Knobler, H. Furukawa, M. O'Keeffe and O. M. Yaghi, *Science*, 2008, **319**, 939–943.
37 J. Zhang, T. Wu, C. Zhou, C. S., P. Feng and X. Bu, *Angew. Chem. Int. Ed.*, 2009, **48**, 2542–2545.
38 Y.-Q. Tian, S.-Y. Yao, D. Gu, K.-H. Cui, D.-W. Guo, G. Zhang, Z.-X. Chen and D.-Y. Zhao, *Chem. Eur. J.*, 2010, **16**, 1137–1141.
39 S. Horike, K. Kadota, T. Itakura, M. Inukai and S. Kitagawa, *Dalton Trans.*, 2015, **44**, 15107–15110.
40 K. Kadota, E. Sivaniah, S. Bureekaew, S. Kitagawa and S. Horike, *Inorg. Chem.*, 2017, **56**, 8744–8747.
41 R. D. Shannon, *Acta Cryst. A*, 1976, **32**, 751–767.
42 E. A. Donlan, H. L. B. Boström, H. S. Geddes, E. M. Reynolds and A. L. Goodwin, *Chem. Comm.*, 2017, **53**, 11233–11236.
43 D. D. Lee and H. S. Seung, *Nature*, 1999, **401**, 788–791.
44 M. W. Berry, M. Brown, A. N. Langville, V. P. Pauca and R. J. Plemmons, *Comp. Stat. Data Anal.*, 2007, **52**, 155–173.
45 N. L. Evans, P. M. M. Thygesen, H. L. B. Boström, E. M. Reynolds, I. E. Collings, A. E. Phillips and A. L. Goodwin, *J. Am. Chem. Soc.*, 2016, **138**, 9393–9396.
46 L. Vegard, *Z. Physik*, 1921, **5**, 17–26.
47 J. M. Newsam, *Science*, 1986, **231**, 1093–1099.
48 Y. Hu, H. Kazemian, S. Rohani, Y. Huang and Y. Song, *Chem. Comm.*, 2011, **47**, 12694–12696.
49 A. Kranjc, T. Kos, N. Zabukovec Logar and G. Mali, *Angew. Chem. Int. Ed.*, 2015, **54**, 10535–10538.
50 K. C. Jayachandrababu, R. J. Verploegh, J. Leisen, R. C. Nieuwendaal, D. S. Sholl and S. Nair, *J. Am. Chem. Soc.*, 2016, **138**, 7325–7336.
51 A. Krajnc, B. Bueken, D. De Vos and G. Mali, *J. Magn. Res.*, 2017, **279**, 22–28.
52 R. L. McGreevy and L. Pusztai, *Mol. Simul.*, 1988, **1**, 359–367.
53 M. T. Dove and H. Fang, *Rep. Prog. Phys.*, 2016, **79**, 066503.
54 D. Dubbeldam, K. S. Walton, D. E. Ellis and R. Q. Snurr, *Angew. Chem. Int. Ed.*, 2007, **46**, 4496–4499.
55 S. S. Han and W. A. Goddard III, *J. Phys. Chem. C*, 2007, **111**, 15185–15191.
56 K. W. Chapman, P. J. Chupas and C. J. Kepert, *J. Am. Chem. Soc.*, 2006, **128**, 7009–7014.
57 E. F. Baxter, T. D. Bennett, A. B. Cairns, N. J. Brownbill, A. L. Goodwin, D. A. Keen, P. A. Chater, F. Blanc and A. K. Cheetham, *Dalton Trans.*, 2016, **45**, 4258–4268.
58 A. L. Goodwin and C. J. Kepert, *Phys. Rev. B*, 2005, **71**, 140301.
59 P. Ding, E. J. Liang, Y. Jia and Z. Y. Du, *J. Phys.: Condens. Matter*, 2008, **20**, 275224.
60 V. E. Fairbank, A. L. Thompson, R. I. Cooper and A. L. Goodwin, *Phys. Rev. B*, 2012, **86**, 104113.
61 R. J. Verploegh, Y. Wu and D. S. Sholl, *Langmuir*, 2017, **33**, 6481–6491.
62 D. A. Keen and A. L. Goodwin, *Nature*, 2015, **521**, 303–309.
63 C. Castillo-Blas, V. A. de la Peña-O'Shea, I. Puente-Orench, J. Romero de Paz, R. Sáez-Puche, E. Gutiérrez-Puebla, F. Gándara and Á. Monge, *Sci. Adv.*, 2017, **3**, e1700773.